THE JOURNAL OF BIOLOGICAL CHEMISTRY
Vol. 279, No. 37, Issue of September 10, pp. 39000–39009, 2004
Printed in U.S.A.

Enzyme-catalyzed Mechanism of Isoniazid Activation in Class I and Class III Peroxidases*

Received for publication, March 3, 2004, and in revised form, June 29, 2004
Published, JBC Papers in Press, July 1, 2004, DOI 10.1074/jbc.M402384200

Roberta Pierattelli‡, Lucia Banci‡, Nigel A. J. Eady§, Jacques Bodiguel¶, Jamie N. Jones§, Peter C. E. Moody‖, Emma Lloyd Raven, Brigitte Jamart-Grégoire¶, and Katherine A. Brown§‡‡**

*From the ‡Dipartimento di Chimica e Centro Risonanze Magnetiche, Universitá di Firenze, Polo Scientifico, Via Luigi Sacconi 6, 50019 Sesto Fiorentino (Florence), Italy, §Department of Biological Sciences, Centre for Molecular Microbiology and Infection, Flowers Building, Imperial College London, London SW7 2AZ, United Kingdom, ¶Laboratoire de Chimie Physique Macromoléculaire, UMR 7568 CNRS-INPL, ENSIC 1, rue Grandville F-54001 Nancy, France, and ‖Department of Biochemistry and **Department of Chemistry, University of Leicester, Leicester LE1 7RH, United Kingdom*

There is an urgent need to understand the mechanism of activation of the frontline anti-tuberculosis drug isoniazid by the *Mycobacterium tuberculosis* catalase-peroxidase. To address this, a combination of NMR spectroscopic, biochemical, and computational methods have been used to obtain a model of the frontline anti-tuberculosis drug isoniazid bound to the active site of the class III peroxidase, horseradish peroxidase C. This information has been used in combination with the new crystal structure of the *M. tuberculosis* catalase-peroxidase to predict the mode of INH binding across the class I heme peroxidase family. An enzyme-catalyzed mechanism for INH activation is proposed that brings together structural, functional, and spectroscopic data from a variety of sources. Collectively, the information not only provides a molecular basis for understanding INH activation by the *M. tuberculosis* catalase-peroxidase but also establishes a new conceptual framework for testing hypotheses regarding the enzyme-catalyzed turnover of this compound in a number of heme peroxidases.

Isoniazid (isonicotinic acid hydrazide, INH)[1] is a prodrug that forms a key part of the frontline chemotherapy used to treat tuberculosis in both developed and developing countries. More than 8 million people per year are diagnosed with tuberculosis, and nearly 2 million of those people die (1). The continued rise in drug-resistant and multidrug-resistant strains of tuberculosis and the scale of the tuberculosis epidemic has stimulated fundamental research to elucidate the molecular mechanisms of anti-tuberculosis drugs, including INH, with a view that this information can initiate the discovery of new antimicrobial targets and alternative treatment regimes.

Although INH has been in clinical use for the treatment of tuberculosis since the 1950s, the mechanism of activation of this prodrug and its mode of action are still not fully established. However, numerous *in vitro* and *in vivo* studies have shown that a catalase-peroxidase (CP), endogenous to *Mycobacterium tuberculosis* (the principal causative agent of the disease), is required for activation of INH (discussed in Ref. 2). This dimeric, heme-containing enzyme of ~160-kDa molecular mass is a member of class I of the superfamily of plant, fungal, and bacterial peroxidases and displays characteristic catalatic and peroxidatic activities (3–5). The latter activity using hydrogen peroxide has been invoked as a means of oxidizing INH (6–8). An additional manganese dependence has also been suggested based on studies using the related *Mycobacterium smegmatis* CP (9, 10), although this activity may not play an essential role in INH oxidation by the *M. tuberculosis* CP (8, 11). However, *M. tuberculosis* CP has been shown to display the ability to oxidize Mn^{2+} as well as halogenated compounds using a chloroperoxidatic activity (12).

The determination of the crystal structure for a recombinant form of *M. tuberculosis* CP (*mt*CP) (2) has been a significant step toward understanding enzyme-catalyzed activation of INH. This structure provides a three-dimensional framework for rationalizing how structural elements within the active site of this enzyme can contribute to drug activation assuming a binding site for INH can be identified. Computational analyses of the *mt*CP structure identified an energetically favorable binding site for INH near the δ-*meso* edge of the heme (2). This location is similar to that observed for other small aromatic compounds in the crystal structures of class I, II, and III peroxidases (13–16). An alternative binding site has also been suggested based upon crystallographic studies of the *Burkholderia pseudomallei* CP, which places INH in a surface loop structure (17) ~10 Å away from the binding site of small aromatic compounds located near the δ-*meso* edge of the heme. The local environment of INH in this surface loop is considerably different from that near the δ-*meso* edge of the heme, and activation of the INH in this case is proposed to involve an electron transfer pathway that would be unique to CP enzymes (17). Presently there is no reported structure of an INH-peroxidase complex, and it is clear that identification of an INH binding site is essential for defining key residues and other structural elements that catalyze the activation of the drug.

Interestingly, it has been shown that the class III peroxidase, horseradish peroxidase (HRP), can oxidize INH using hydrogen peroxide in a classic peroxidatic mechanism involving the for-

* This work was supported by Commission of European Communities Contract BMH4-CT96-1492, Florence Large Scale Facility PARABIO Contract HPRI-CT-2001-00147, Consiglio Nazionale delle Ricerche-Progetto Finalizzato Biotecnologie Grant 97.01027.49, the United Kingdom Biotechnology and Biological Sciences Research Council, the American Society for Engineering Education, and the Wellcome Trust. The costs of publication of this article were defrayed in part by the payment of page charges. This article must therefore be hereby marked "*advertisement*" in accordance with 18 U.S.C. Section 1734 solely to indicate this fact.

‡‡ To whom correspondence should be addressed. Tel.: 44-20-75945298; Fax: 44-20-75945207; E-mail: k.brown@imperial.ac.uk.

[1] The abbreviations used are: INH, isonicotinic acid hydrazide (isoniazid); CP, catalase-peroxidase; *mt*CP, *M. tuberculosis* catalase-peroxidase; HRPC, horseradish peroxidase (HRP) C; APX, ascorbate peroxidase; CcP, cytochrome *c* peroxidase; rsAPX, recombinant soybean ascorbate peroxidase; rpAPX, recombinant pea ascorbate peroxidase; BHA, benzhydroxamic acid; NOESY, nuclear Overhauser effect (NOE) spectroscopy; HPLC, high performance liquid chromatography; *t*-BuOOH, *tert*-butyl hydroperoxide.

mation of Compound I to produce reactive species capable of reducing nitro blue tetrazolium (18). Later work from the same group demonstrated similar activity using partially purified *M. tuberculosis* CP (6). Studies have shown that Compound II can be stably generated in the reaction of HRP Compound I with INH, further supporting the operation of a classic peroxidatic mechanism of INH oxidation for this enzyme (19). The same authors also identified Compound I in the reaction of *M. tuberculosis* CP with INH and speculated that a similar peroxidatic pathway may be utilized (19). Based upon these data and the amenability of HRP to characterization of enzyme-aromatic compound complexes using NMR methods (20–28), we have, therefore, undertaken a high resolution NMR characterization of the interactions between horseradish peroxidase C (HRPC) and INH. This paper, therefore, presents models of the HRPC·INH complex in the presence and absence of cyanide. Using ^{15}N-labeled INH, we demonstrate that HRPC activates INH via the splitting of a C-N bond as previously reported for *mt*CP (8). In addition, we report data demonstrating that other class I enzymes, ascorbate peroxidase (APX) and cytochrome *c* peroxidase (CcP), are also capable of turning over INH. Furthermore, the availability of an NMR-derived HRPC·INH complex enables us to generate docked complexes of INH in the active sites of the crystal structures of APX (29) and CcP (30) in the same manner as described for the *mt*CP·INH complex (2). Using these complexes potential enzyme-drug interactions found in the class I and class III peroxidases are described, and an enzyme-catalyzed mechanism for INH activation is proposed.

EXPERIMENTAL PROCEDURES

Materials—Deuterium oxide, 3-nitrobenzoic acid and hydrogen peroxide (30% w/v) were obtained from Sigma-Aldrich. HRPC was also obtained from Sigma Aldrich and was used without any further purification. Protein concentration of HRPC was determined spectrophotometerically by measuring absorbance at 403 nm (ϵ_{403} = 102,000 M^{-1} cm^{-1}) (31). *mt*CP was prepared as described in Bertrand *et al.* (2). Recombinant soybean APX (rsAPX) and recombinant pea APX (rpAPX) were prepared as described previously (32). Hydroxylamine HCl was from Fluka (Gillingham, UK) and was recrystallized in ethanol before use. KCN was from Carlo Erba (Milan, Italy), and INH was obtained from Cairn Chemicals (Chesham, UK). Singly labeled isotopic isomers of INH were prepared as previously described (33, 34). All other chemicals were obtained from Merck.

NMR Spectroscopy—Samples were prepared by exchanging HRPC into 50 mM NaH_2PO_4 buffer in either H_2O (buffer A) or deuterium oxide (buffer B) using a Centricon-10 (Amicon, Danvers, MA) and then adjusting the pH to 7.0. The cyanide adduct was obtained by the addition of excess solid KCN followed by re-adjusting the pH to 7.0. Protein concentration of samples prepared in buffer A ranged from 0.4 to 0.8 mM, whereas the protein concentration of samples prepared in buffer B was 2.5 mM.

One-dimensional ^{1}H NMR and titration experiments were performed using a standard water-suppression sequence at 318 K using either a Bruker DRX 500 or a Bruker AVANCE 800 spectrometer. Spectra for HRPC in buffer A were collected at 500 MHz, whereas spectra for the HRPC-cyanide adduct in buffer B were collected at 800 MHz. Titration of INH into both samples was performed by the stepwise addition using 1.0, 0.5, 0.25, 0.1, and 0.01 M stock solutions of INH (prepared in buffer A or B) until no further change in the spectra were observed (>250 mM).

Two-dimensional NMR experiments including NOESY (35) and clean total correlation spectroscopy (36) spectra were collected using a Bruker AVANCE 800 spectrometer at both 318 and 308 K. T_1 values of the INH signals from solutions containing 20 mM INH in buffer B and concentrations of HRPC or the HRPC-cyanide adduct from 0 to 0.8 mM in buffer B were recorded at 800 MHz using the inversion recovery sequence (37). All two-dimensional NMR experiments were phase-sensitive, recorded in the time proportional phase increment mode (38) using standard pulse sequences. For NOESY experiments, spectral widths of 50,000 and 20,000 Hz were used with mixing times of 20 and 50 ms and recycle delays ranging from 300 to 500 ms. For scalar experiments only the smallest spectral width was used with a recycle delay of 500 ms. Spectra were acquired using 800–1024 free induction decays with 4096 complex data points. Data were processed using a sine-squared bell function shifted 45° or 30°. Data-matrices were 0-filled to give the final 4096 × 2048-processed maps.

Data were analyzed using the XEASY program (ETH, Zurich, Switzerland) (39) on an IBM RISC 6000. NOESY cross-peaks were integrated with the standard routines of the XEASY program and translated in proton-proton distances using cross-peaks between protons at fixed distances for calibration.

Analysis of Relaxation Data—The observed longitudinal relaxation time of a nucleus belonging to a molecule exchanging between the bound and free state and concomitantly sensing the paramagnetic metal ion is, in the fast-exchange limit, the weighted average between the diamagnetic ($T_{1\,d}$) and paramagnetic ($T_{1\,M}$) rates according to

$$T_{1\,obs}{}^{-1} = f_b\, T_{1\,M}{}^{-1} + f_f\, T_{1\,d}{}^{-1} \qquad \text{(Eq. 1)}$$

where f_b is the molar fraction of nuclei bound to the paramagnetic molecule, and f_f is the unbound molar fraction. For molecules with low affinity for the paramagnetic molecule, the former quantity can safely be approximated to unity. If the affinity constant for the adduct or complex is known, from the value of $T_{1\,M}{}^{-1}$ it is possible to obtain a distance limit between the metal ion and the nucleus according to the Solomon-Bloembergen equation (40, 41). For INH binding to HRPC, $T_{1\,obs}$ of interest are those of the ring proton resonances of INH that can easily be measured at various concentrations of enzyme. Because the pyridinyl ring is symmetrical but does flip, INH C2H protons are defined as the ring carbons in the *ortho* position relative to pyridinyl nitrogen, whereas INH C3H protons are in the *meta* position (Fig. 1*A*). A reasonable estimate of the diamagnetic contribution $T_{1\,d}$ can be obtained from the T_1 values of the same resonances in the presence of the HRPC-cyanide adduct, provided that INH binds to this adduct in a manner similar to that which it binds HRPC. This assumption is reasonable because the iron in the HRPC-cyanide adduct is in a low spin state and, therefore, has much faster electronic relaxation rates compared with unliganded HRPC. It follows that nuclear relaxation rates for the cyanide adduct are much less affected by the paramagnetic center.

Molecular Dynamics Simulations—Before molecular dynamics simulations, models of HRPC, the HRPC-cyanide adduct, HRPC·INH, and HRPC-cyanide-INH were constructed using the modeling program Sybyl (Tripos Associates, Inc.) on an Evans and Sutherland model PS390 graphics work station. The starting model for HRPC was the x-ray structure (42) (Protein Data Bank code 1ATJ). Residues reported in the x-ray structure were used in the modeling studies. Cyanide was docked on to the HRPC model by coordinating its carbon atom to the HRPC iron at an orientation essentially perpendicular to the heme plane based upon coordinates of the x-ray structure for the CcP-cyanide complex (43). The orientation of INH in HRPC·INH and HRPC-cyanide-INH models was obtained using distances derived from relaxation data and/or NOEs as described above. All models also contained the two calcium ions present in the HRPC crystal structure.

Molecular dynamics simulations were carried out on the four models listed above with the AMBER 4.1 software package (44) using an IBM/SP2 parallel computer. Throughout the calculations the SHAKE algorithm was used (45), and geometrical restraints were applied to maintain the four disulfide bridges in the HRPC crystal structure (Cys-11–Cys-91, Cys-44–Cys-49, Cys-97–Cys-301, and Cys-177–Cys-209). All force field parameters (except those for the heme, the proximal histidine residue, calcium ions, and cyanide) were taken from the AMBER 4.1 force field data base (46) optimized for molecular dynamics simulations of proteins with the inclusion of water molecules. Force field parameters for INH were derived from the parameters of its composite moieties also contained in the AMBER 4.1 force field data base (46). Atomic point charges for INH were kindly provided by Dr. Caterina Ghio (ICQEM-CNR, Pisa, Italy) and were obtained from GAUSSIAN 94 (47) using the 6–31G basis set with geometry optimization. Equilibrium bond lengths and angles for the heme and proximal histidine were taken from the crystallographic coordinates of the HRPC structure (42), and similar parameters for the cyanide ligand were used from previously published data (48). Force constants for bond stretching and bending and torsional force constants used in the calculations for the heme, the proximal histidine residue, calcium ions, and cyanide were identical to those previously described (48–50).

The overall charge of HRPC was neutralized by adding chloride counterions using the CION utility in AMBER 4.1. This was done by placing counterions near positively charged residues and avoiding the channel region near the heme. All four models were then solvated with a 10-Å shell of Monte Carlo T1P3P water molecules (51) using the

SOL-BLOB option in the EDIT module of AMBER 4.1. Counterions and solvent water molecules were equilibrated by minimizing the root mean square energy gradient to 0.10 kcal $mol^{-1}Å^{-1}$ followed by 5 ps of molecular dynamics calculations. Energy minimization of the entire system (for all four models) was then performed until a root mean square energy gradient of 0.10 kcal $mol^{-1}Å^{-1}$ was obtained. Energy-minimized models at 0 K were heated to 300 K by performing three molecular dynamics calculations of 3 ps each at 100, 200, and 300 K in that order. The coupling with the external bath was maintained using a coupling constant of 0.1 ps. Finally, a 121.5-ps trajectory was calculated for all models. Averaged structures, generated by the CARNAL module of AMBER 4.1, were obtained using the last 67.5 ps of the trajectory. These structures were then minimized to obtain representative models in solution.

Computational Predictions of INH Binding Sites—GRID calculations (52) were performed on atomic coordinate files of the crystal structures of APX (53) and CcP (30). INH was docked into the active site of the crystal structures of rsAPX (29) and CcP (30) based upon a superposition of each of these crystal structures with the HRPC·INH NMR-derived model using all atoms of the heme moiety, the conserved distal histidine and arginine residues, and the conserved proximal histidine and aspartic acid residues. Superpositions were carried out using Swiss PDB Viewer (54). Generation of the *mt*CP-INH model was done in a similar manner as described (2).

Protein Production and Purification—Purification of CcP was undertaken using a modified literature protocol (55, 56). 4 × 20 ml of LB containing 100 μg/ml ampicillin were inoculated with one colony from an L-agar plate containing 100 μg/ml ampicillin streaked from a glycerol stock of *Escherichia coli* BL21-CODONPLUS(*DE3*)-RIL[pT7CCP-Zf1] (56). After overnight growth at 37 °C with shaking, each 20-ml culture was inoculated into 1 liter of 2× YT containing 100 μg/ml of ampicillin. Cells were grown at 37 °C with shaking until a cell density corresponding to an A_{600} of 0.8 was reached. IPTG was then added to a final concentration of 0.4 mM, and growth was allowed to continue for a further 18 h at 33 °C. Cells were harvested by centrifugation at 6000 × *g* at 4 °C for 45 min. Cell pellets were routinely stored at −20 °C.

Frozen cells were thawed and resuspended in 15 ml of 50 mM KH_2PO_4/K_2HPO_4, pH 6.0, containing 1 mM EDTA. At this stage reconstitution with heme was performed according to the protocol previously described (2). Cells were lysed by sonication with 3 × 30-s bursts on power level 8 using a microtip and an XL2020 sonicator (Labcaire Systems, Clevedon, UK). Insoluble material was removed by centrifugation at 9000 × *g* at 4 °C for 1 h. The resulting supernatant was treated with 100 μg/ml DNase and 10 μg/ml RNase for 1 h at 4 °C and then recentrifuged as before.

A two-step purification protocol was followed using a DEAE-Sepharose anion exchange column (50 mM KH_2PO_4/K_2HPO_4, pH 6.0, 1 mM EDTA with 0–1 M NaCl gradient) and an Amersham Biosciences HiLoad 16/60 Superdex 200 prep grade gel filtration column (50 mM KH_2PO_4/K_2HPO_4, pH 6.0, 1 mM EDTA, 0.15 M NaCl) as described for *mt*CP (2).

Reaction Product Analysis—The procedures described for identification of reaction products from INH turnover are based upon similar studies undertaken for *mt*CP (8). Reactions were carried out in 50 mM Na_2HPO_4, pH 7.5, at 37 °C. Incubations to assess INH turnover contained 2 μM enzyme and 200 μM INH in either the presence or absence of 10 mM *tert*-butyl hydroperoxide (*t*-BuOOH) in a total volume of 1 ml. After incubation, 250-μl aliquots were removed at 30, 60, and 180 min. Reaction mixtures containing labeled INH consisted of 0.1 μM HRPC, 200 μM singly labeled $^{14}N,^{15}N$ or $^{15}N,^{14}N$ isomers of INH, and 10 μM H_2O_2 in a total volume of 1 ml. Reactions were incubated overnight at 37 °C. In each case, enzyme was subsequently removed by ultrafiltration, and the filtrate was incubated at 37 °C for 20 min with a solution of 0.13 M NH_2OH, pH 6.8, containing 3-nitrobenzoic acid (as an external standard) before HPLC analysis.

HPLC separations were performed on a Waters-600 system using a Macherey-Nagel EC 250–4 NUCLEODUR 100–5 C18 ec (5 μm) column. The mobile phase was acetonitrile, 50 mM ammonium acetate, pH 7.0, at a flow rate of 1 ml/min, and reaction products were eluted using isocratic conditions (5/95). Separations for reaction assays containing *t*-BuOOH were performed using a linear gradient. Products were identified by comparison with authentic samples, and concentrations were determined by integration of HPLC profiles (monitored at 260 nm) along with a comparison of the peak obtained for the external standard, 3-nitrobenzoic acid. Aldehyde was detected as the oxime. To assess the incorporation of ^{15}N into the amide oxidation product, solvent was removed from the isonicotinamide fraction, and the resulting residue was dissolved in ethanol then analyzed using a Fisons GC8000/MD800 mass spectrometer equipped with a 15 m × 0.250-mm column in the positive electronic impact mode.

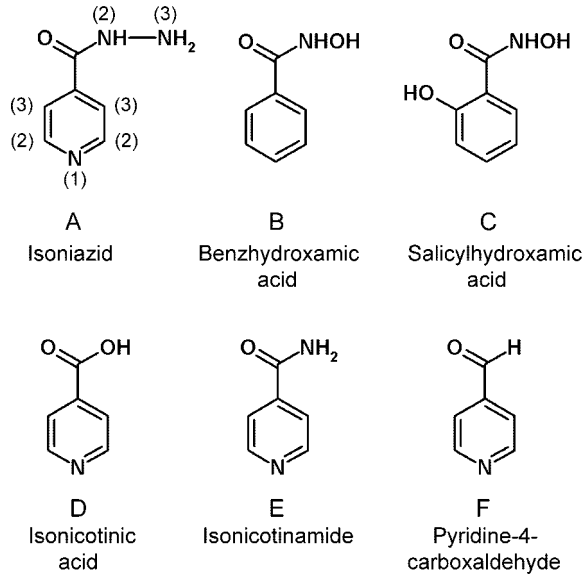

FIG. 1. **Structures of aromatic and pyridinyl compounds.** *A*, INH. *B*, BHA. *C*, salicylhydroxamic acid. Shown are oxidation products of INH isonicotinic acid (*D*), isonicotinamide (*E*), pyridine-4-carboxaldehyde (*F*).

RESULTS AND DISCUSSION

Affinity of INH for HRPC—Numerous studies of HRP have shown that this enzyme is able to catalyze the oxidation of a variety of aromatic donor compounds using the classic peroxidatic cycle involving the formation of Compounds I and II (for review, see Dunford *et al.* (21)). This mechanism was also invoked to describe the oxidation of INH (Fig. 1*A*) by HRP (19). ^1H NMR spectra of HRPC and the HRPC-cyanide adduct in the absence and presence of INH are shown in Figs. 2 and 3, respectively. Titration of HRPC with INH yielded an apparent equilibrium affinity constant (K_A) of 84.0 ± 0.5 M^{-1} corresponding to a calculated apparent K_D value ($1/K_A$) of 11.9 mM, which is slightly higher compared with reported values obtained using isothermal titration methods, 1.1–3.4 mM (57), and may simply reflect subtle differences between the two techniques. Titration of the HRPC-cyanide complex with INH yielded a similar K_A of 70.9 ± 0.4 M^{-1}, corresponding to a K_D of 14.1 mM, suggesting that the hydrazinyl moiety of INH has a similar binding site in the presence and absence of cyanide and that INH is not directly coordinated to the heme.

The INH·HRPC Complex—Previous assignments of signals for the HRPC-cyanide adduct (28) enabled comparative analysis of spectra obtained from two dimensional-NOESY experiments of this complex in the absence and presence of INH. A selective perturbation of the ^1H NMR spectrum for the HRPC-cyanide adduct is observed upon the addition of INH (Fig. 3 and Table I) but does not indicate the presence of any large conformational changes associated with INH binding to the enzyme. Residues most affected include Arg-38, Phe-41, His-42, and Gly-169 with smaller perturbations observed for Phe-152 and Phe-172. Notably, signals of Phe-179 are somewhat obscured by overlapping INH C3H ring resonances. Dipole-dipole couplings between the INH C2H protons and the $C18H_3$ and $C17^{1a}H$ protons of the heme (Fig. 4) are clearly observed as well as a weak NOE connectivity between the INH C3H and the His42 Cϵ1H protons (Fig. 5). A few other dipole-dipole couplings between INH and the HRPC-cyanide adduct can also be observed, but resonances associated with the latter are unassigned. Additionally, titration of 20 mM INH with increasing

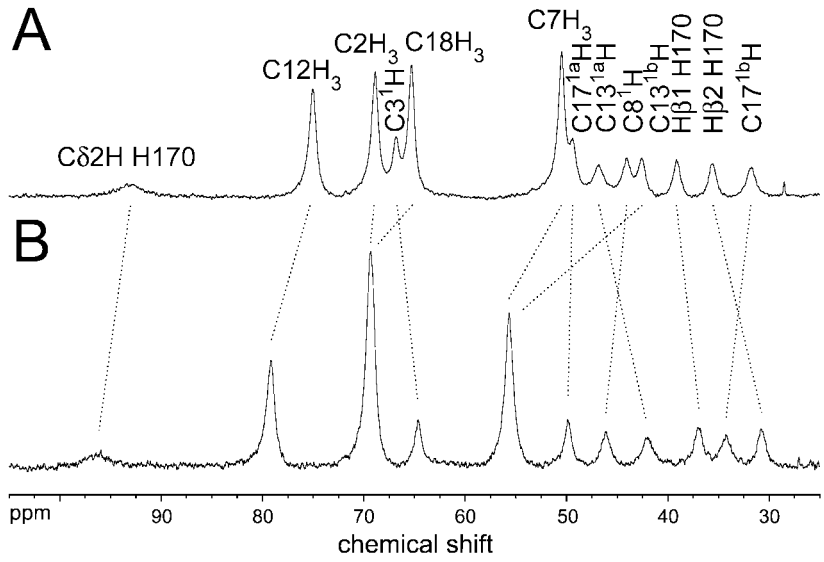

FIG. 2. **Comparison of the effects of INH upon the 500 MHz ^{1}H NMR spectra of HRPC at 318 K.** *A*, HRPC resting state (0.6 mM). *B*, HRPC in the presence of 270 mM INH. Assignment of resonances for HRPC are indicated in the *top trace*, and *dotted lines* connect identical resonances between the two spectra shown.

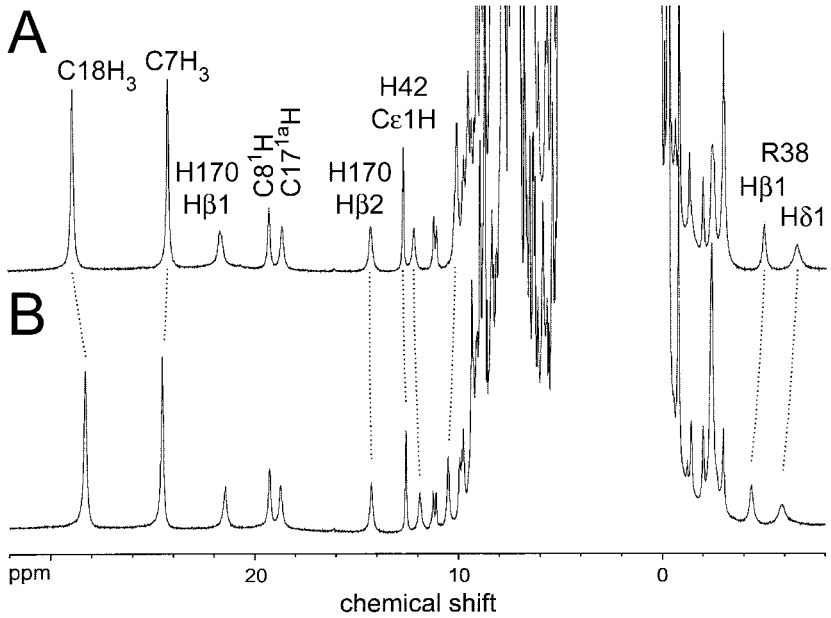

FIG. 3. **Comparison of the effects of INH upon the 800 MHz ^{1}H NMR spectra of the HRPC-cyanide adduct at 318 K.** *A*, HRPC-cyanide low spin adduct (2.5 mM). *B*, HRPC-cyanide in the presence of 10 mM INH. Assignment of resonances for HRPC are indicated in the *top trace*, and *dotted lines* connect identical resonances between the two spectra shown.

amounts of HRPC (up to a concentration of 0.8 mM) led to a reduction of the $T_{1\,obs}$ values for C2H and C3H ring protons of INH, from 8.7 and 7.1 s to 3.4 and 1.2 s, respectively. The low spin HRPC-cyanide adduct was used as a reference value for the diamagnetic species (as the paramagnetic contribution to $T_{1\,obs}$ of INH resonances produced by the HRPC-cyanide adduct is small compared with that of the high spin HRPC). This resulted in lower distance limits of separation for contacts between the INH C2H or C3H protons and the heme iron of 7.1 and 5.4 Å, respectively.

The crystallographic coordinates of unliganded HRPC (42), in the presence and absence of a docked cyanide ligand, were used as a starting point for molecular dynamic calculations. These calculations yielded solution equilibrated models of HRPC and the HRPC-cyanide adduct, which showed only minor deviations from the crystal structure (root mean square deviation of 0.9–1.0 Å for backbone atoms and 1.2–1.3 Å for side chains). All secondary structure elements as well as other key structural features, including the four disulfide bridges, two calcium ion binding sites, and the heme binding site, remained intact. In addition, water molecules placed in a 10-Å shell surrounding HRPC were observed to minimize at "conserved" positions in the active site of the x-ray structure, near the heme C20 and iron in the distal pocket. Models of the HRPC·INH and HRPC-cyanide-INH complexes, generated without explicit constraints on the position of INH, yielded positions of INH in both these complexes that were consistent with experimental data obtained from the NOEs.

The proposed modes of binding for INH to the HRPC-cyanide adduct and to HRPC are shown in Fig. 6, *A* and *B*. INH occupies the same region of the active site in a similar orientation to that seen in the crystal structure of HRPC with the structurally similar benzhydroxamic acid (BHA; Fig. 1*B* and Fig. 6*C*) (16). Comparison of the crystal structure of HRPC·BHA (16) and the NMR-based model of HRPC·INH demonstrates that both BHA and INH can access a similar but not identical set of interactions that may relate to their differing affinities (Fig. 6*D*). The pyridinyl moiety of INH is located in a hydrophobic "aromatic binding pocket" (25), near the heme-18 methyl and makes a number of non-bonded contacts to residues including Gly-69, Ala-140, Pro-141, and Phe-179 as well as to the heme itself. In the HRPC·INH and HRPC-cyanide-INH models the hydrazide moiety of INH forms hydrogen bonds to a backbone carbonyl oxygen, INH N3-Pro-139 O (2.7–2.8 Å), and to the distal cata-

TABLE I

Summary of proton assignments in the ^1H NMR spectrum for HRPC-cyanide and HRPC-cyanide-INH complexes (10 mM INH) at 318 K in 50 mM NaH_2PO_4 buffer, pH 7.0, in D_2O

Entries under HRPC-cyanide-INH_f are the values extrapolated for the fully formed adduct.

Residue	Assignment	HRPC-cyanide δ	HRPC-cyanide-INH δ	HRPC-cyanide-INH_f δ
		ppm	*ppm*	*ppm*
Heme	$C2H_3$	2.84	2.49	1.96
	$C3^1H$	5.27	5.39	5.57
	$C3^2H$	−1.33	−1.43	−1.58
	$C3^2H$	-2.40	−2.46	−2.55
	$C7H_3$	24.22	24.51	24.95
	$C8^1H$	19.24	19.24	19.24
	$C8^2H$	−2.98	−3.03	−3.11
	$C8^2H$	−2.00	−2.04	−2.10
	$C12H_3$	6.54	6.56	6.59
	$C13^{2a}H$	−2.52	−2.43	−2.29
	$C17^{1a}H$	18.64	18.70	18.79
	$C17^{1b}H'$	9.59	9.79	10.09
	$C17^{2a}H$	2.61	2.54	2.43
	$C17^{2b}H'$	0.53	0.56	0.61
	$C18H_3$	28.89	28.29	27.38
Arg-38	HN	5.64	5.84	6.14
	Hα	0.56	1.17	2.10
	Hβ1	−4.96	−4.41	−3.57
	Hβ2	−0.62	−0.26	0.29
	Hγ1	0.65	1.18	1.99
	Hγ2	−1.41	Not located	
	Hδ1	−6.55	−5.90	−4.91
	Hδ2	0.94	1.18	1.54
Phe-41	Hδ1,2	7.56	7.99	8.64
	Hε1,2	6.31	5.88	5.23
	Hβ2	2.68	2.97	3.41
His-42	HN	9.12	9.34	9.67
	Hα	4.73	4.72	4.70
	Hδ1	16.04	16.09	16.17
	Hδ2	10.06	10.49	11.14
	Hε1	12.68	12.54	12.33
Phe-152	Hζ or Hδ1,2	5.44	5.40	5.34
	Hε1,2	6.26	6.23	6.18
	Hδ1,2 or Hζ	7.13	7.10	7.05
Ser-167	Hα	5.70	5.66	5.60
	Hβ	3.24	3.11	2.91
Gly-169	HN	10.12	9.93	9.64
	Hα	5.73	5.40	4.90
	Hα'	5.01	4.80	4.48
His-170	HN	12.21	11.86	11.33
	Hα	9.51	8.97	8.15
	Hβ1	21.65	21.43	21.10
	Hβ2	14.31	14.26	14.18
	Hδ2	20.7	19.6	17.9
	Hε1	−27.0	−25.1	−22.2
Thr-171	HN	9.08	8.93	8.70
Phe-172	HN	9.52	9.34	9.07
	Hδ1,2	7.62	7.50	7.32
	Hε1,2	7.16	7.08	6.96
	Hζ	6.55	6.51	6.45
Ile-244	δ1CH_3	−2.99	−2.42	−1.55
	Hγ1	0.11	0.25	0.46
	Hγ2	1.10	1.29	1.50
Phe-45	Hδ1,2 or Hζ	4.81	4.80	4.78
	Hε1,2	6.37	6.35	6.32
	Hζ or Hδ1,2	6.99	6.97	6.94

lytic histidine residue, INH O-His-42 Nε2 (3.0 Å). In the HRPC·INH model (Fig. 6*B*) the INH carbonyl oxygen also forms a hydrogen bond (2.7 Å) to the conserved water located directly above heme iron in the distal pocket but not to the side chain of Arg-38, as would be predicted from the HRPC-BHA crystal structure (16). This is probably due to the high mobility observed for this group in the molecular dynamic simulations. The lack of an interaction may be an artifact of this calculation but may also suggest that this interaction is somewhat weaker compared with others in this particular complex. Flexibility of this residue has been observed in the active site of CcP (43). In addition, in comparative thermodynamic studies of HRPC the flexibility of Arg-38 has been implicated to play a role in reducing affinities for certain aromatic hydroxamic acid analogues compared with BHA (57). In contrast, the INH carbonyl oxygen in the HRPC-cyanide-INH model (Fig. 6*A*) does appear to form a hydrogen bond with the Arg-38 Nη2 group (2.9 Å) and may also interact with the nitrile group of the cyanide ligand (3.1 Å); however, the significance of these differences may only be small given the similarities in the affinities for INH of the HRPC and HRPC-cyanide complexes.

Predicted INH Binding Site in Class I Peroxidases—The NMR-generated model of the HRPC·INH complex is shown in Fig. 7*A*. A predicted binding mode of the drug is shown in the crystal structures of *mt*CP (Fig. 7*B*) (2), rsAPX (Fig. 7*C*) (29), and CcP (Fig. 7*D*) (30), based upon superpositions between the

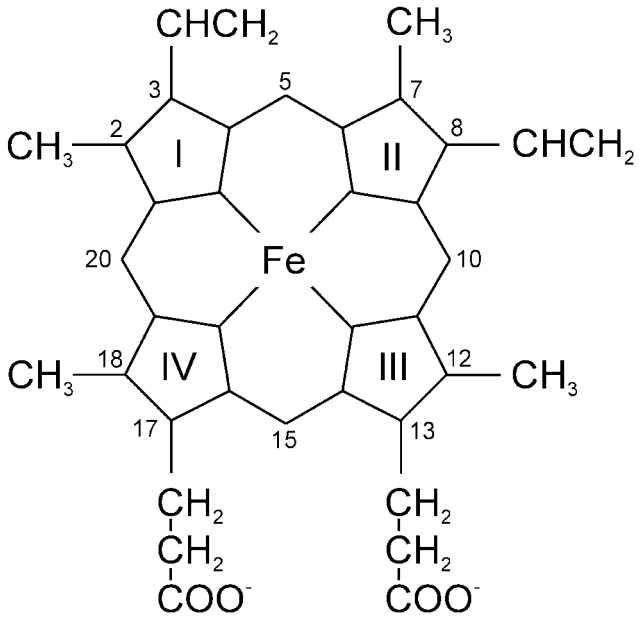

FIG. 4. **Structure of iron protoporphyrin IX.** The numbering used in this paper is shown.

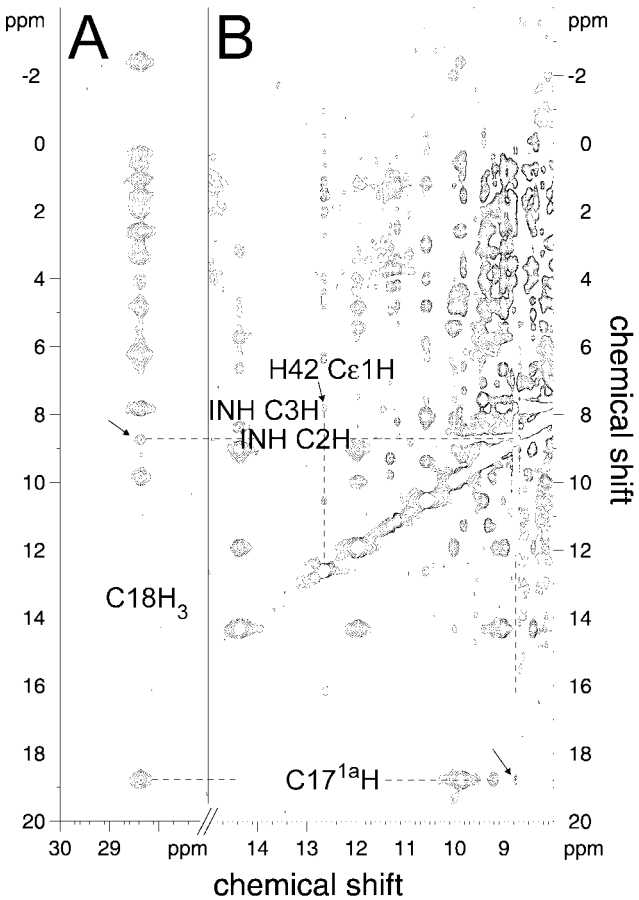

FIG. 5. **Two-dimensional NOESY spectrum of the HRPC-cyanide complex with INH, collected at 318 K, with a mixing time of 50 ms.** Region *A* includes values from 30 to 27 ppm, whereas region *B* includes values from 15 to 8 ppm. *Dotted lines* are drawn to show the frequencies of NOESY peaks, which are indicated by *arrows*, between HRPC-cyanide and INH resonances.

coordinates of these class I enzymes and the HRPC·INH complex. Location of this common binding site for the drug, oriented near the δ-*meso* edge of the heme, is consistent with computational predictions that identify this region as the most favorable binding site in both *mt*CP and HRPC (2). In rsAPX and CcP, the predicted binding mode of INH in these class I enzymes overlaps with both the GRID interaction maps, which show this site to be the most favored for INH binding as well as the position of salicylhydroxamic acid (Fig. 1*C*) in the recent APX-salicylhydroxamic acid crystal structure (13). Notably, based upon the crystal structure of *B. pseudomallei* CP, an alternative binding site has been proposed (17) that, in the *mt*CP crystal structure, is located in a surface loop of the enzyme (2). However, as discussed in Bertrand *et al.* (2), the region near the δ-*meso* edge is suggested to be the most favored site for INH binding in *mt*CP and is consistent with the location of INH in the HRPC·INH complexes presented here (Fig. 6, *A* and *B*).

Closer inspection of the predicted binding modes of INH in the class I peroxidases shows that several common structural features shared with HRPC may play key roles in INH binding. These include the distal histidine residue, which is common to all these enzymes, the ligating water molecule, and the backbone carbonyl groups of Pro-132 and Pro-145 in the rsAPX (29) and CcP (30) structures, respectively (Fig. 7, *C* and *D*). These carbonyl groups may interact with N3 of INH as seen in the HRPC·INH NMR models (Fig. 6, *A* and *B*). In addition, the conserved distal tryptophan residue, (*e.g.* Trp-107 in *mt*CP crystal structure; Fig. 7*B*) also has the potential to form contacts with N3 of INH. Utilization of the main-chain carbonyl group of Pro-132 and the side chain of Trp-41 for binding a related compound, salicylhydroxamic acid (Fig. 1*C*), have also been reported in the crystal structure of the complex of salicylhydroxamic acid with rsAPX (13). However, the carboxylic acid moiety of Asp-137 in *mt*CP, which is conserved among CP homologues, has the potential to form interactions with both the N3 and/or the N1 group of INH (Fig. 7*B*). In HRPC, a water molecule (*w313*) occupies the equivalent position (Fig. 7*A*). In rsAPX (Fig. 7*C*) and CcP (Fig. 7*D*) this site is occluded somewhat by residues Ala-70 and Ser-81, respectively. It is also interesting to note that the predicted binding mode of INH in the class I peroxidases, based upon superpositions with the NMR-derived INH coordinates in HRPC, does not suggest that the drug will ligate to the heme. In the case of *mt*CP, this orientation of INH is also consistent with spectroscopic data, which indicate that the enzyme is in the 5-coordinate state when the drug is bound (58–60).

Enzyme-catalyzed Mechanism for INH Activation—Previous studies of *mt*CP demonstrated that incubation of INH with the enzyme and H_2O_2 resulted in small but increasing amounts of the acid (Fig. 1*D*) and amide (Fig. 1*E*) derivatives of INH as well as the production of the pyridine-4-carboxaldehyde aldehyde derivative (Fig. 1*F*), all as a function of time (7, 8). As shown in Table II, HRPC as well as the class I peroxidases rsAPX, rpAPX, and CcP are all capable of turning over INH, producing acid and amide reaction product with varying efficiencies. Given the similarities the active sites of these enzymes share with *mt*CP (discussed in Ref. 2), these data further support the proposal that a common site located near the δ-*meso* edge of the heme (Fig. 7) is used for INH binding and activation.

A proposed reaction mechanism for the activation of INH leading to the generation of the activated acyl radical and the production of the amide end product via a diazene intermediate is shown in Fig. 8*A* (8). Using $^{14}N,^{15}N$ or $^{15}N,^{14}N$ isomers of INH, singly labeled at the hydrazide moiety, the level of incorporation of label into the amide end product was determined using HPLC and electrospray mass spectrometry methods. In the case of *mt*CP, the amide reaction product obtained con-

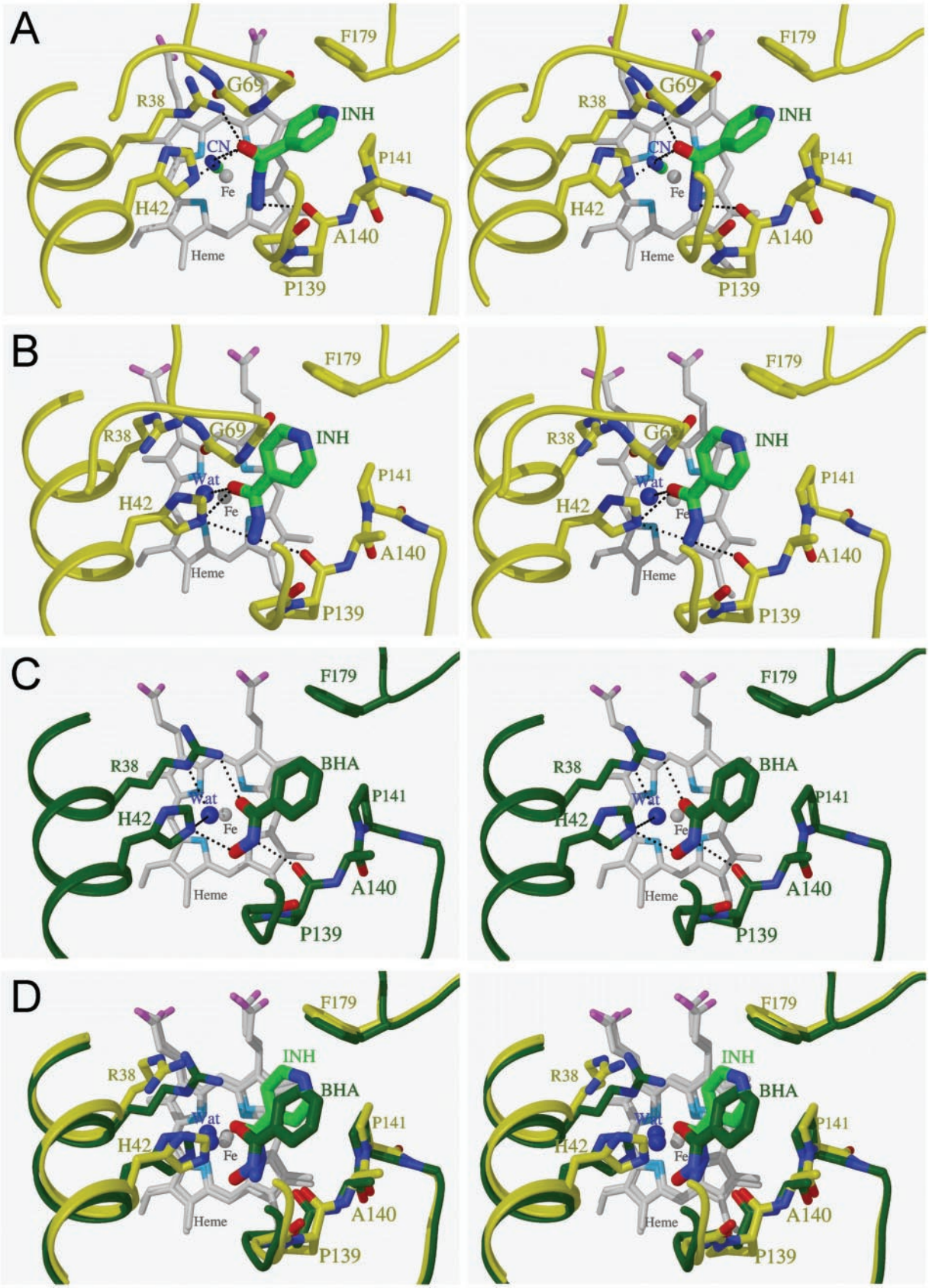

FIG. 6. **Stereodiagrams of compounds bound to the active site of HRPC.** *A*, HRPC-cyanide-INH. *B*, HRPC·INH. *C*, HRPC·BHA. *D*, overlay of HRPC·INH with HRPC·BHA. In all panels the heme (in *gray*) and protein main chains and side chains are depicted in *yellow* (for the NMR models of INH complexes) or *dark green* (for the x-ray coordinates of the HRPC-BHA complex) (16). *Wat* in *panels B–D* refers to the conserved water molecule located on the distal side of the active site above the heme (listed as HOH 999 in the RCSB Protein Data Bank, code 2ATJ). Carbon atoms of INH are shown in *light green* (*panels A*, *B*, and *D*), whereas carbon atoms of BHA are shown in *dark green* (*panels C* and *D*). Interactions of INH and/or BHA with cyanide or with possible hydrogen bonding groups in the active site of HRPC are shown by *dotted lines* (*panels A–C*). This figure was produced using BOBSCRIPT (63).

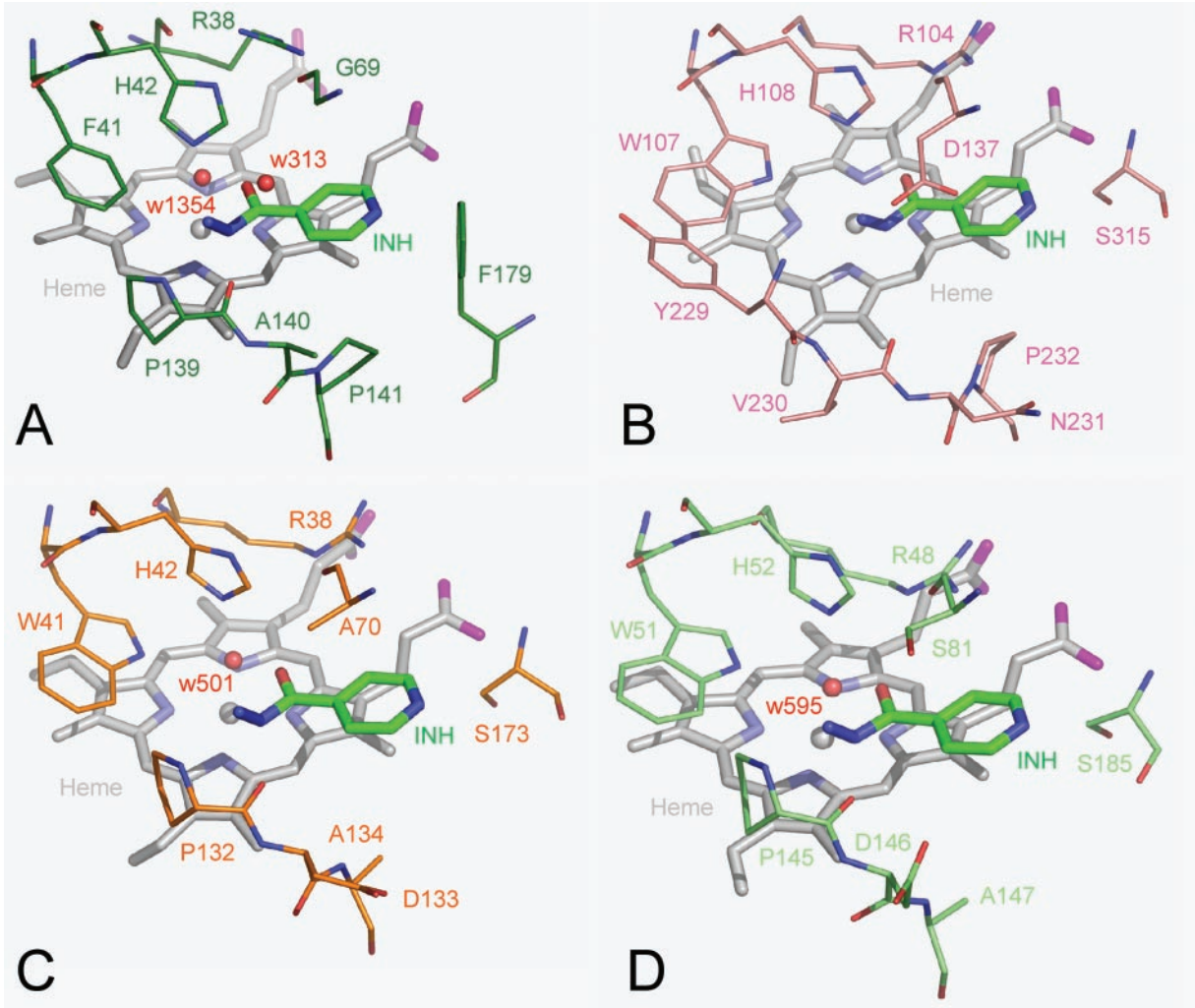

FIG. 7. **HRPC·INH complex generated from NMR and INH docked into the active sites of class I peroxidases.** *A*, HRPC·INH. *B*, *mt*CP·INH. *C*, rsAPX·INH. *D*, CcP·INH. In all panels the heme is in *gray*. Protein main chains and side chains are depicted in *dark green* for the HRPC NMR model of INH complex, *pink* for the *mt*CP crystal structure (2), *orange* for the APX crystal structure (29), and *light green* for the CcP crystal structure (30). The conserved water molecule on the distal side of the active site *above* the *heme* is shown in *red* (*w1354* for HRPC, *w501* for APX, and *w595* for CcP). A water molecule in HRPC (w313), which occupies a similar position to one of the oxygen atoms of Asp-137 in *mt*CP, is shown in *panel A*. Carbon atoms of INH are shown in *green*. This figure was produced using PyMOL (Ref. 64; www.pymol.org).

TABLE II
INH oxidation catalyzed by class I and class III peroxidases
Reactions were carried out in 50 mM Na_2HPO_4 buffer, pH 7.5, at 37 °C. In each case, 2 μM enzyme, 200 μM INH, and 10 mM *t*-BuOOH.were used.

Reaction	INH			Acid			Amide			Aldehyde		
	30 min	60 min	180 min	30 min	60 min	180 min	30 min	60 min	180 min	30 min	60 min	180 min
		μM			μM			μM			μM	
INH alone	200	200	200	0	0	0	0	0	0	0	0	0
*mt*CP/INH/*t*-BuOOH	38	16	1	130	150	159	10	12	9.6	5.2	5.7	5.1
CcP/INH/*t*-BuOOH	135	130	134	42	42	46	5.1	3.9	5.2	0	0	0
rsAPX/INH/*t*-BuOOH	163	120	117	54	57	62	3.1	3.2	3.2	3.1	1.3	1.9
rpAPX/INH/*t*-BuOOH	118	135	130	35	44	49	2.2	3.3	3.5	0	2.3	2.1
HRPC/INH/*t*-BuOOH	68	44	12	88	122	152	3.8	4	4.8	0	0	0

tained 50% of the ^{15}N label, which was interpreted as arising from a splitting of the C-N bond of INH (Fig. 1*A*) (8) rather than N-N splitting of the hydrazide as previously proposed (7). Identical levels of ^{15}N label incorporation were obtained here using HRPC, suggesting that HRPC and *mt*CP share a similar mechanism of activation of INH, including the pathway, which results in formation of the amide reaction product. Based upon these findings and given the similarities in the active sites of HRPC, *mt*CP, rsAPX, and CcP (Fig. 7), an enzyme-catalyzed mechanism for INH activation can be proposed.

Fig. 8*B* indicates how interactions between structural elements of the active site could stabilize intermediates on the activation pathway of INH in *mt*CP, resulting in the production of the acyl radical. In the first step shown, Compound I, generated after reaction with peroxide, is reduced by INH in a single electron transfer to the heme. In concert, a proton is lost from the hydrazide moiety and could be accepted by His-108. In the second step of the reaction, the C-N bond of the hydrazide is split, yielding diazene. The acyl radical may diffuse from the active site or may remain oriented near the δ-*meso* edge of the heme. The diazene reaction intermediate may be stabilized in the active site of the enzyme by interactions with Trp-107,

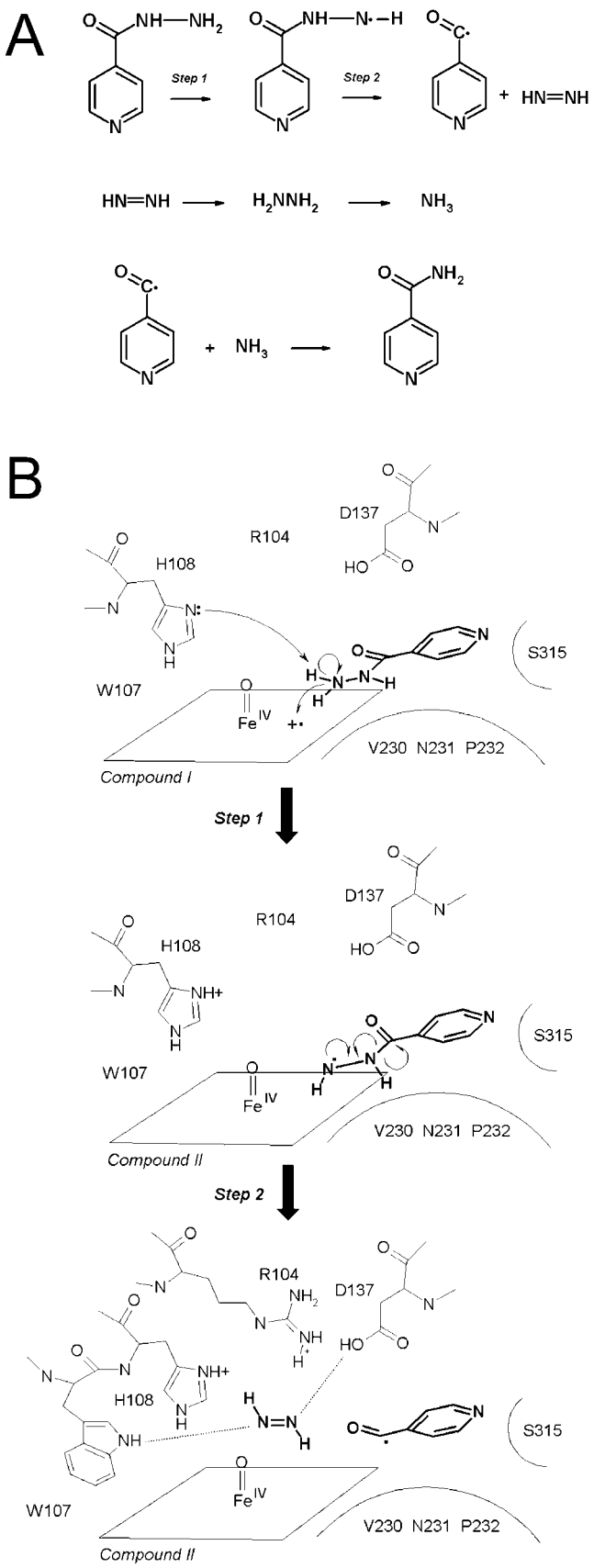

FIG. 8. **Proposed reaction mechanism for oxidation of INH in *mt*CP active site.** *A*, proposed reaction mechanism for production of isonicotinamide (8). *B*, *mt*CP residues potentially involved in production of isonicotinoyl radical. Possible interactions are shown with *dotted lines*. The heme porphyrin is represented by a *rhombus*.

Asp-137, and even the oxyferryl group in the same manner as suggested for hydrogen peroxide in the catalatic reaction (61). Transformation of diazene to hydrazine and ammonia (Fig. 8*A*) may involve deprotonation of the His-108 and Asp-137 side chains in *mt*CP, although Arg-104 also has the possibility of providing a proton given its proximity, its proposed conformational mobility (43, 62), and its role as an "entropic gate keeper" (57). As discussed previously in the analysis of the INH binding site in other peroxidases, which are capable of activating the drug, the Asp-137 residue is not a conserved feature (2). In HRPC (Fig. 7*A*) a water molecule, Wat313, occupies a similar position to the carboxylic acid moiety of Asp-137 (Fig. 7*B*). The ability of Wat313 to occupy this position is due at least in part to the presence of Gly-69, which creates a space large enough to be filled by a well ordered solvent molecule. In APX (Fig. 7*C*) and CcP (Fig. 7*D*), Asp-137 is replaced by Ala-70 or Ser-81, respectively, which partially occludes this pocket, preventing a water molecule from occupying a similar position to Wat313 of HRPC. The presence of Asp-137, which is conserved in CPs, may help to explain why INH is turned over most rapidly by *mt*CP when compared with the other peroxidases under study here. In HRPC, which turns over INH at a reduced rate, the position of the carboxylic acid group of Asp-137 in *mt*CP is occupied by Wat-313, which may not protonate diazene as efficiently. APX and CcP, which turn over INH most slowly, do not have a water molecule occupying that position and may, thus, rely upon other solvent molecules in the active site or even residues such as the distal arginine (equivalent to Arg-104 in Fig. 8*B*) to provide protons for the transformation of diazene to ammonia. Ammonia may also be oriented by similar interactions shown for the diazene (Fig. 8*B*) before the proposed attack by the acyl radical to generate the amide reaction product (Fig. 8*A*).

To conclude, we have utilized a combination of spectroscopic, biochemical, and computational techniques to obtain a model of INH bound to the active site of HRPC. Furthermore, we have utilized information about the HRPC·INH complex in combination with crystal structures of *mt*CP (2) and the class I peroxidases APX (13, 29) and CcP (30) to predict the binding mode of INH in these enzymes, which have all been shown to turnover the drug. Using available mechanistic data about the activation pathway involving the formation of the isonicotinamide end product (8), we propose an enzyme-catalyzed mechanism for INH activation that can yield the acyl radical thought to be the activated form of the drug. We, therefore, propose that the models of the enzyme-INH complexes presented here provide a structural framework for further studies designed to test hypotheses regarding *in vitro* and *in vivo* activation of INH.

Acknowledgments—We thank Tony Cass, Judit Nagy, Jesmin, and Jeremy Baum for useful discussions in the preparation of this manuscript and Liz Carpenter and Thomas Bertrand for help in the preparation of figures. In addition, we also thank Paolo Carloni for useful discussions regarding the molecular dynamics calculations, Caterina Ghio for allowing us to use the Gaussian 94 program for point charge calculations of isoniazid, Andy Smith for providing coordinates of the x-ray structure of HRPC, and Tom Poulos for providing x-ray coordinates of the CcP-cyanide complex.

REFERENCES

1. Dye, C., Scheele, S., Dolin, P., Pathania, V., and Raviglione, M. C. (1999) *J. Am. Med. Assoc.* **282,** 677–686
2. Bertrand, T., Eady, N. A. J., Jones, J. N., Jesmin, Nagy, J. M., Jamart-Gregoire, B., Raven, E. L., and Brown, K. A. (2004) *J. Biol. Chem.* **279,** 38991–38999
3. Winder, F. G., and Collins, P. B. (1970) *J. Gen. Microbiol.* **63,** 41–48
4. Nagy, J. M., Cass, A. E. G., and Brown, K. A. (1997) *J. Biol. Chem.* **272,** 31265–31271
5. Johnsson, K., Froland, W. A., and Schultz, P. G. (1997) *J. Biol. Chem.* **272,** 2834–2840
6. Shoeb, H. A., Bowman, B. U., Jr., Ottolenghi, A. C., and Merola, A. J. (1985) *Antimicrob. Agents Chemother.* **27,** 404–407

7. Johnsson, K., and Schultz, P. G. (1994) *J. Am. Chem. Soc.* **116,** 7425–7426
8. Bodiguel, J., Nagy, J. M., Brown, K. A., and Jamart-Gregoire, B. (2001) *J. Am. Chem. Soc.* **123,** 3832–3833
9. Magliozzo, R. S., and Marcinkeviciene, J. A. (1996) *J. Am. Chem. Soc.* **118,** 11303–11304
10. Magliozzo, R. S., and Marcinkeviciene, J. A. (1997) *J. Biol. Chem.* **272,** 8867–8870
11. Lei, B., Wei, C. J., and Tu, S. C. (2000) *J. Biol. Chem.* **275,** 2520–2526
12. Jakopitsch, C., Regelsberger, G., Furtmuller, P. G., Ruker, F., Peschek, G. A., and Obinger, C. (2001) *Biochem. Biophys. Res. Commun.* **287,** 682–687
13. Sharp, K. H., Moody, P. C. E., Brown, K. A., and Raven, E. L. (2004) *Biochemistry*, 8644–8651
14. Itakura, H., Oda, Y., and Fukuyama, K. (1997) *FEBS Lett.* **412,** 107–110
15. Tsukamoto, K., Itakura, H., Sato, K., Fukuyama, K., Miura, S., Takahashi, S., Ikezawa, H., and Hosoya, T. (1999) *Biochemistry* **38,** 12558–12568
16. Henriksen, A., Schuller, D. J., Meno, K., Welinder, K. G., Smith, A. T., and Gajhede, H. (1998) *Biochemistry* **37,** 8054–8060
17. Carpena, X., Loprasert, S., Mongkolsuk, S., Switala, J., Loewen, P. C., and Fita, I. (2003) *J. Mol. Biol.* **327,** 475–489
18. Shoeb, H. A., Jr., B. U. B., Ottolenghi, A. C., and Merola, A. J. (1985) *Antimicrob. Agents Chemother.* **27,** 399–407
19. Chouchane, S., Lippai, I., and Magliozzo, R. S. (2000) *Biochemistry* **39,** 9975–9983
20. Veitch, N. C., and Williams, R. J. P. (1990) *Eur. J. Biochem.* **189,** 351–362
21. Dunford, H. B. (1991) in *Peroxidases in Chemistry and Biology* (Everse, J., and Grisham, M. B., eds) pp. 1–24, CRC Press, Inc., Boca Raton, FL
22. Veitch, N. C., and Williams, R. J. P. (1991) in *Biochemical, Molecular, and Physiological Aspects of Plant Peroxidases* (Lobarzewski, J., Greppin, H., Penel, C., and Gaspar, T. H., eds) pp. 99–109, University of Geneva, Geneva
23. Banci, L., Bertini, I., Bini, T., Tein, M., and Turano, P. (1993) *Biochemistry* **32,** 5825–5831
24. Mar, G. N. L., Chen, Z., Vyas, K., and McPherson, A. D. (1995) *J. Am. Chem. Soc.* **117,** 411–419
25. Veitch, N. C. (1995) *Biochem. Soc. Trans.* **23,** 232–240
26. Veitch, N. C., Gao, Y., Smith, A. T., and White, C. G. (1997) *Biochemistry* **36,** 14751–14761
27. Smith, A. T., and Veitch, N. C. (1998) *Curr. Opin. Chem. Biol.* **2,** 269–278
28. Ropp, J. S. D., Mandal, P. K., and Mar, G. N. L. (1999) *Biochemistry* **38,** 1077–1086
29. Sharp, K. H., Mewies, M., Moody, P. C., and Raven, E. L. (2003) *Nat. Struct. Biol.* **10,** 303–307
30. Wang, J. M., Mauro, M., Edwards, S. L., Oatley, S. J., Fishel, L. A., Ashford, V. A., Xuong, N. H., and Kraut, J. (1990) *Biochemistry* **29,** 7160–7173
31. Aibara, S., Yamashita, H., Mori, E., Kata, M., and Morita, Y. (1982) *J. Biochem.* (*Tokyo*) **92,** 531–539
32. Lad, L., Mewies, M., and Raven, E. L. (2002) *Biochemistry* **41,** 13774–13781
33. Brosse, N., Pinto, M. F., and Jamart-Gregoire, B. (1998) *J. Chem. Soc. Perkin Trans. I*, 3685–3688
34. Jamart-Gregoire, B., Brosse, N., and Bodiguel, J. (1998) *J. Synthesis* 269–270
35. Macura, S., Wuthrich, K., and Ernst, R. R. (1982) *J. Magn. Reson.* **47,** 351–357
36. Bax, A., Caldwell, J. W., and Davis, D. G. (1985) *J. Magn. Reson.* **65,** 355–360
37. Vold, R. L., Waugh, J. S., Klein, M. P., and Phelps, D. E. (1968) *J. Chem. Phys.* **48,** 3831–3832
38. Marion, D., and Wuthrich, K. (1983) *Biochem. Biophys. Res. Commun.* **113,** 967–974
39. Eccles, C., Guntert, P., Billeter, M., and Wuthrich, K. (1991) *J. Biomol. NMR* **1,** 111–130
40. Solomon, I. (1955) *Phys. Rev.* **99,** 559–565
41. Bloembergen, N. (1957) *J. Chem. Phys.* **27,** 572–573
42. Gajhede, M., Schuller, D. J., Henriksen, A., Smith, A. T., and Poulos, T. L. (1997) *Nat. Struct. Biol.* **4,** 1032–1038
43. Edwards, S. L., and Poulos, T. L. (1990) *J. Biol. Chem.* **265,** 2588–2595
44. Pearlman, D. A., Case, D. A., Caldwell, J. W., Ross, W. S., Cheatham, T. E., Ferguson, D. M., Seibel, G. L., Singh, U. C., Weiner, P. K., and Kollman, P. A. (1995) AMBER 4.1 Ed., University of California, San Francisco
45. van Gunsteren, W. F., and Berendsen, H. J. C. (1977) *Mol. Physiol.* **34,** 1311–1327
46. Cornell, W. D., Cieplak, P., Bayly, C. I., Gould, I. R., Jr., Merz, K. M., Ferguson, D. M., Spellmeyer, D. C., Fox, T., Caldwell, J. W., and Kollman, P. A. (1995) *J. Am. Chem. Soc.* **117,** 5179–5197
47. Fritsch, M. J., Trucks, G. W., Schlegel, H. B., Gill, P. M. W., Johnson, B. G., Robb, M. A., Cheeseman, J. R., Keith, T., Petersson, G. A., Montgomery, J. A., Raghavachari, K., Al-Laham, M. A., Zakrzewski, V. G., Ortiz, J. V., Foresman, J. B., Cioslowski, J., Stefanov, B. B., Nanayakkara, A., Challacombe, M., Peng, C. Y., Ayala, P. Y., Chen, W., Wong, M. W., Andres, J. L., Replogle, E. S., Gomperts, R., Martin, R. L., Fox, D. J., Binkley, J. S., Defrees, D. J., Baker, J., Stewart, J. P., Head-Gordon, M., Gonzalez, C., and Pople, J. A. (1995) GAUSSIAN 94, Revision B., 3 Ed., Gaussian, Inc., Pittsburg, PA
48. Banci, L., Bertini, I., Bren, K. L., Gray, H. B., Sompornpisut, P., and Turano, P. (1995) *Biochemistry* **34,** 11385–11398
49. Banci, L., Carloni, P., and Savellini, G. G. (1994) *Biochemistry* **33,** 12356–12366
50. Banci, L., Carloni, P., Diaz, A., and Savellini, G. G. (1996) *J. Biol. Inorg. Chem.* **1,** 264–272
51. Jorgensen, W. L., Chandrasekhar, J., Madura, J., Impey, R. W., and Klein, M. L. (1983) *J. Chem. Phys.* **79,** 926–935
52. Goodford, P. J. (1985) *J. Med. Chem.* **28,** 849–857
53. Patterson, W. R., and Poulos, T. L. (1995) *Biochemistry* **34,** 4331–4341
54. Guex, N., and Peitsch, M. C. (1997) *Electrophoresis* **18,** 2714–2723
55. Fishel, L. A., Villafranca, J. E., Mauro, J. M., and Kraut, J. (1987) *Biochemistry* **26,** 351–360
56. Darwish, K., Li, H. Y., and Poulos, T. L. (1991) *Protein Eng.* **4,** 701–708
57. Aitken, S. M., Turnbull, J. L., Percival, M. D., and English, A. M. (2001) *Biochemistry* **40,** 13980–13989
58. Chouchane, S., Girotto, S., Kapetanaki, S., Schelvis, J. P., Yu, S., and Magliozzo, R. S. (2003) *J. Biol. Chem.* **278,** 8154–8162
59. Kapetanaki, S., Chouchane, S., Girotto, S., Yu, S., Magliozzo, R. S., and Schelvis, J. P. (2003) *Biochemistry* **42,** 3835–3845
60. Wengenack, N. L., Todorovic, S., Yu, L., and Rusnak, F. (1998) *Biochemistry* **37,** 15825–15834
61. Jakopitsch, C., Auer, M., Regelsberger, G., Jantschko, W., Furtmuller, P. G., Ruker, F., and Obinger, C. (2003) *Biochemistry* **42,** 5292–5300
62. Bonagura, C. A., Bhaskar, B., Shimizu, H., Li, H., Sundaramoorthy, M., McRee, D. E., Goodin, D. B., and Poulos, T. L. (2003) *Biochemistry* **42,** 5600–5608
63. Esnouf, R. M. (1997) *J. Mol. Graphics Model* **15,** 132–134
64. DeLano, W. L. (2002) *The PyMOL Molecular Graphics System*, DeLano Scientific, San Carlos, CA

Enzyme-catalyzed Mechanism of Isoniazid Activation in Class I and Class III Peroxidases

Roberta Pierattelli, Lucia Banci, Nigel A. J. Eady, Jacques Bodiguel, Jamie N. Jones, Peter C. E. Moody, Emma Lloyd Raven, Brigitte Jamart-Grégoire and Katherine A. Brown

J. Biol. Chem. 2004, 279:39000-39009.
doi: 10.1074/jbc.M402384200 originally published online July 1, 2004
